CARBON 64 (2013) 158–169

Available at www.sciencedirect.com

ScienceDirect

journal homepage: www.elsevier.com/locate/carbon

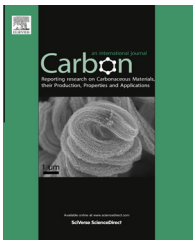

Large-scale and low cost synthesis of graphene as high capacity anode materials for lithium-ion batteries

Shuangqiang Chen [a], *Peite Bao* [b], *Linda Xiao* [a], *Guoxiu Wang* [a,*]

[a] *Centre for Clean Energy Technology, School of Chemistry and Forensic Science, University of Technology, Sydney, NSW 2007, Australia*
[b] *School of Physics, The University of Sydney, NSW 2006, Australia*

ARTICLE INFO

Article history:
Received 19 June 2013
Accepted 19 July 2013
Available online 24 July 2013

ABSTRACT

Graphene has emerged as an intriguing and attractive functional material for a wide range of applications, owing to its unique physical, chemical and mechanical properties. Herein, we report large-scale production of high quality single crystalline graphene sheets based on the ambient pressure chemical vapor deposition (APCVD) method using acetylene (C_2H_2) as the carbon source and coral-like iron with body-centered-cubic structure as the catalyst. The process can be scaled up for large quantity production at a low cost. The optimum APCVD temperature has been identified to be 850 °C, which is much lower than that catalyzed by other metals. Transmission electron microscopy (TEM), atomic force microscopy, Raman spectroscopy and X-ray photoemission spectroscopy characterizations show the single crystalline and high quality nature of the as-prepared graphene produced by the bottom-up APCVD approach. A new horizontal "dissolution–deposition–growth" mechanism is proposed and verified by high resolution TEM. When applied as anode materials in lithium ion batteries, graphene sheets exhibited a high lithium storage capacity and an excellent cyclability. The capability of preparing crystalline graphene on a large scale with low cost opens an avenue for technological applications of graphene in many fields.

1. Introduction

Since its discovery in 2004, graphene [1], a monolayer of carbon atoms with sp^2 bonds, has attracted intensive investigations world-wide. Many fascinating applications for graphene have been proposed, including electronics [2–4], super-strong composite materials, energy storage and conversion [5–7], molecular sensing and bio-medicine etc. [8,9]. Large-scale production of high quality graphene materials is critical to realize these applications. Graphene nanosheets have been prepared by micromechanical cleavage and chemical vapor deposition (CVD) growth on transition metal (Cu, Fe, Co, Ni) or noble metal (Ru, Pt) substrates [10–24]. Although gram-scale graphene materials have been produced through chemical methods such as modified Hummer method [25–29] and organic solvent dispersion method [30], these processes are labor intensive and involve in using toxic, corrosive or volatile chemicals. Longitudinal cutting of carbon nanotubes by plasma etching is also a good optional choice to achieve graphene with desired shape and size [31–34]. Among all previously reported techniques [11,15,35–38], CVD is regarded as a facile approach to prepare graphene in large quantities. Polycrystalline graphene films, four or six-lobe graphene flowers and hexagonally-shaped graphene grains have been prepared on Cu foils by several groups [13], [39–43]. However, it was found that the growth of graphene on

* *Corresponding author.*
E-mail address: Guoxiu.Wang@uts.edu.au (G. Wang).
0008-6223/$ - see front matter
http://dx.doi.org/10.1016/j.carbon.2013.07.048

Cu is self-limited. Monolayer or few-layer graphene and three-dimension graphene foam are also successfully deposited on nickel substrate (including Ni foam) [15,44]. Driven by the "surface-catalysis-deposition" mechanism originated from the continuous connection of carbon fragments on the metal surface or the "dissolution–segregation–deposition" mechanism occurred through the segregation of absorbed carbon atoms at high temperature to metal surface and formation of graphene on cooling [20,42,45,46], maximum size of graphene grown on Cu, Co, Ni, Pt and Ru seldom exceeds the boundaries of the metal substrates [15,39,47–50]. Recently, electrochemical delamination has been reported to recycle metal substrates, demonstrating that copper foil can only be oxidized and consumed less than 40 nm during each growth-delamination-transfer cycle [51]. Repeated growth and bubbling transfer of graphene with millimeter-size using platinum as catalyst was reported by Cheng's group without any loss of Pt substrate [52]. The approaches capable to produce large quantity graphene must be developed to meet other demands of applications such as energy storage and conversion, molecular sensing and bio-medicine. Therefore, synthesis of high quality, large quantity and single crystalline graphene remains a considerable challenge.

Graphene has been investigated and applied as anode materials for lithium ion batteries, demonstrating enhanced capacity and increased high rate performance [6,53]. Graphene-based composites (Sn, Si, Ge, Co_3O_4, Fe_2O_3, NiO and MnO_2 etc.,) also exhibited improved specific capacity and cyclablity when used as anode materials in lithium ion batteries [28,29,54–62]. Inspired by the massive production of carbon nanotubes through the CVD method, we have developed an ambient pressure CVD (APCVD) process to produce graphene sheets on coral-like iron in gram-scale using a bottom-up strategy. The graphene growth is catalyzed by iron, which is similar to the production of carbon nanotubes. We proposed a new growth mechanism called "dissolution–deposition–growth". Differing from other transition metals, iron atoms arrange themselves into two stable crystal structures at different temperatures: the body-centered cubic structure (bcc structure, stable at 1394 °C or above and 912 °C or below, ferrite) and the face-centered cubic structure (fcc structure, stable between 912 and 1394 °C, austenite) [63,64]. Several factors including the concentration of carbon sources, growth time, morphologies and properties of substrates, pressure and cooling rate jointly affect the quality of graphene. Other research groups have demonstrated that graphene can be obtained by ambient pressure CVD or low pressure CVD method using Fe foils or films prepared by conventional magnetron sputtering method with varied thickness [21,65–67], confirming that graphene with few layers can grow on Fe foils or films because the lattice constant of Fe (2.86 Å) is closed to that of graphene (2.46 Å) [21]. We found that the growth of graphene catalyzed by iron is not limited in the boundary of catalysts, leading to large-scale production. Herein, we report the large scale synthesis of graphene by the APCVD method using acetylene as carbon sources. The optimum temperature for the production of graphene has been determined. The major advantages of the process are low cost (using acetylene and iron), high quality of the product (single crystalline) and scalable for large quantity production (1 g graphene can be produced using 100 mg coral-like Fe catalysts).

2. Experimental

2.1. Preparation of catalysts

Fe_2O_3 nanoparticles were prepared by the chemical precipitation method. In a typical synthesis process, Iron nitrate nonahydrate (0.05 mol L^{-1}, 100 mL) was added into urea aqueous solution (1 mol L^{-1}, 100 mL) with magnetic stirring for 30 min. The as-obtained solution was kept at 102 °C under continuous magnetic stirring for 9 h in a 500 mL flask (equipped with a reflux condenser) in ambient atmosphere. Then the brownish red precipitation product was filtered and dried in a vacuum oven overnight at 95 °C. The dry precursor was grounded into fine powders with an agate mortar and dispersed in ethanol with 1 h ultrasonic treatment. After then, the suspension of Fe_2O_3 was dropped on silicon wafers. Finally, the Fe_2O_3 silicon wafers were dried overnight at 95 °C.

2.2. Synthesis of graphene

In order to identify the optimum APCVD growth temperature and time, APCVD were carried out at 550, 650, 750, 825, 850, 875, 900 and 950 °C, respectively, in a horizontal tube furnace. The furnace was heated at a rate of 5 °C·min^{-1} to the designated temperatures under flowing H_2/Ar (H_2: 5%, 400 sccm (standard cubic centimeter per minute)) and kept for 2 h. Before cooling to room temperature, the C_2H_2/Ar gas (C_2H_2: 10%, 50 sccm) was introduced into the quartz tube. After the identification of the optimum temperature (850 °C), APCVD was performed for different time durations: 5 min, 10 min, 30 min and 120 min at 850 °C.

2.3. Materials characterisation

The as-prepared graphene products were characterised by X-ray diffraction (XRD, Rigaku D/max-2550 V with Cu Kα radiation) operated at 40 kV and 30 mA. Raman spectra were measured using a Renishaw inVia Raman spectrometer system (Gloucestershire, UK) equipped with a Leica DMLB microscope (Wetzlar, Germany) and a 17 mW at 633 nm renishaw helium neon laser with 50% power. Atomic force microscopy (AFM) measurements were performed on Dimension 3100 SPM with a tapping mode. The Brunauer–Emmett–Teller (BET) surface area was calculated using experimental points at a relative pressure of P/P^0 = 0.05–0.25. The pore size distribution was derived from the desorption branch using the Barret–Joyner–Halenda (BJH) method. The morphologies and crystal structure of graphene sheets were analyzed by a field emission scanning electron microscope (FE-SEM, JSM-6700F, 20 kV) and transmission electron microscope/selected area electron diffraction (TEM/SAED, JEOL JEM-200CX and JEM-2010F) equipped with an energy-dispersive X-ray spectroscopy (EDX). A thermogravimetric analyser (TGA, SDT 2960) was used to measure the weight percentage of graphene. X-ray photoemission spectroscopy (XPS) was measured by ESCALAB220i-XL (VG Scientific) system with a standard high

vacuum at 2×10^{-9} mbar and a monocharomatic aluminium Kα source. Fourier Transform Infrared (FTIR) Spectra were obtained by Nicolet Magna 6700 FTIR spectrometer. Graphene sheets (1.5 g) were compressed into a round cylinder (at least 10 mm in height). The electrical conductivity was measured using a four-point probe method using a model 2000 6½-digit Keithley Multimeter.

2.4. Electrochemical measurements

The working electrodes were made from 80 wt% of active materials, 10 wt% of the conductive agent (acetylene black), and 10 wt% of the binder (polyvinylidene difluoride). The mixture was stirred by an adjustable high-speed electric agitator. The working electrodes were dried in a vacuum oven. CR2032 coin cells were assembled in an argon-filled glove box (Mbraun, Unilab, Germany), in which both the moisture and oxygen contents were controlled to be less than 0.1 ppm. Lithium foil was used as the counter electrode. The electrolyte (Zhangjiagang Guotai–Huarong New Chemical Materials Co., Ltd.) was 1 M $LiPF_6$ in a 1:1 (weight ratio) mixture of ethylene carbonate and diethyl carbonate. Electrochemical measurements were performed using a LAND-CT2001C battery test system. The cells were discharged and charged galvanostatically in the fixed voltage range of 0.005–3.0 V with a current density of 74.4 mA g^{-1} (0.1C). Higher current rates (0.5C, 1C, 5C and 10C) were also used to test the electrochemical performance. Cyclic voltammetry was measured on a CHI 660D electrochemical workstation at a scan rate of 0.5 mV S^{-1}.

3. Results and discussion

As described in the experimental section, large quantities of graphene have been synthesized at 850 °C by APCVD using a mixture gas of acetylene and argon. The growth of graphene sheets was catalyzed by coral-like iron particles. The as-grown graphene products can be easily harvested by dissolving iron catalysts in hot hydrochloric acid, then washed with copious de-ionized water and dried in a vacuum oven. An example of the as-synthesized products (about 1 g) is shown Fig. 1a and an application of a luminous light emitting diode powered by three cell batteries connected in series with as-prepared graphene as the anode material is also presented in Fig. 1b, which can keep luminous for 5 days. The field emission scanning electron microscope (FESEM) image of coral-like iron catalysts covered by transparent graphene sheets can be easily observed in Fig. 1c. Obviously, graphene sheets grow across the catalyst' boundaries and extend to blank and broad domains. The previous reported growth mechanisms both "surface–catalysis–deposition" and "dissolution—segregation–deposition" cannot well explain this phenomenon. Therefore, a new growth mechanism must be developed to explain the growth process. Fig. 1d shows the SEM image of graphene sheets with a size of approximate 40 μm^2, which contains some winkles associated with the difference of the thermal expansion coefficient between graphene and Fe during cooling. In the first step of the synthesis, Fe_2O_3 nanoparticles (about 20 nm) were firstly prepared by a urea-assisted precipitation method. During deposition, Fe_2O_3

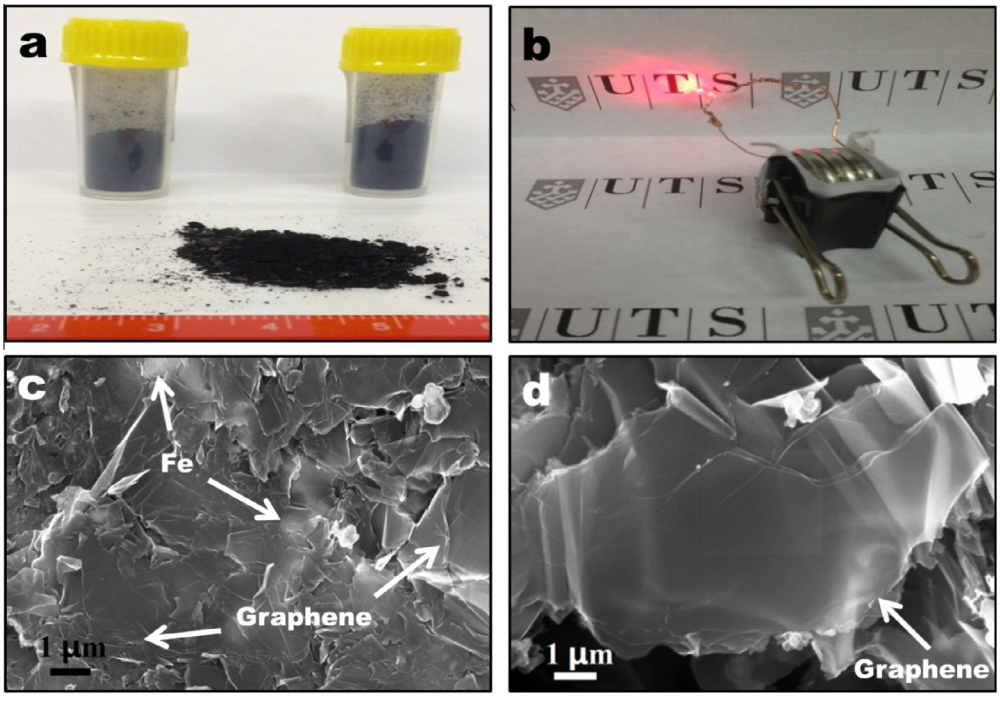

Fig. 1 – (a) Example of graphene in large quantity (about 1 g) produced by APCVD method using C_2H_2 as the carbon source and Fe as the catalyst. (b) A luminous light-emitting diode powered by three coin cells connected in series with graphene electrode as the anode material. (c) FESEM images of the as-prepared graphene sheets with coral-like Fe particles. (d) Graphene sheets after the removal of iron catalysts.

nanoparticles were reduced to Fe and form coral-like porous iron networks (Fig. S1a and b).

We explored the influences of temperature and growth time on the APCVD deposition products. Aiming to generate iron nanoparticles and complete the structure transformation of iron at the specific temperature, Fe_2O_3 nanoparticles were firstly reduced to Fe in H_2 for 2 h. As the volume of Fe_2O_3 is larger than that of Fe, the space of Fe nanoparticles occupied will shrink during the reduction process. When APCVD was carried out at 550 °C, carbon nanofibers (CNF) catalyzed by Fe nanoparticles with diameters less than 20 nm were obtained (Fig. 2) [68], which could be ascribed to the "tip-growth" mechanism [69–71]. Fe particles were anchored on the tips of CNFs, more details are shown in supporting information

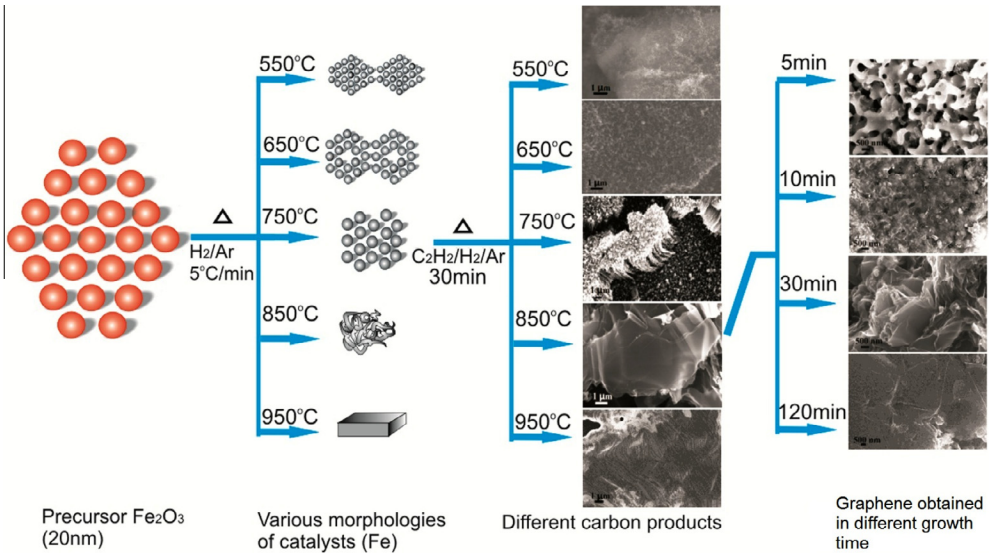

Fig. 2 – The schematic diagram for the synthesis of graphene and other carbon materials (including carbon nanofibers, carbon nanotubes, vertically alligned carbon nanotubes and graphite) at different temperatures and different growth time.

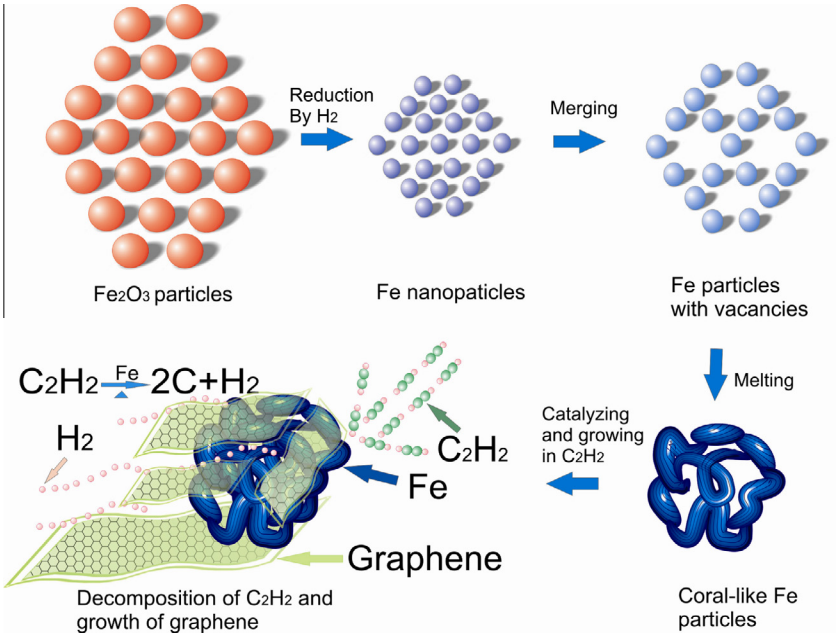

Fig. 3 – Schematic illustration of the "dissolution–deposition–growth" mechanism. Fe_2O_3 nanoparticles (about 20 nm) were reduced by H_2 for 2 h and shrank to Fe nanoparticles. Affected by heat treatments, Fe particles are shrunk, merged and melted with the increase of temperature. The acetylene firstly diffuses on Fe surface (body-centered-cubic structure) and decomposes to active carbon atoms and hydrogen atoms. Once carbon concentration absorbed in the lattice of Fe reached the maximum value, active carbon atoms merge along outside of Fe particles, form hexagonal structure, and gradually grow into graphene sheets. With the assistance of high-energy hydrogen atoms and continuous supply of acetylene, large-size and gram-scale graphene sheets can be produced, which is called "dissolution–deposition–growth" mechanism.

(Figs. S2a and S3a–c). As the temperature was increased to 650 °C, carbon nanotubes were formed (Fig. 2). With the "tip-growth" mechanism, open-ended CNT can be observed in supporting information (Figs. S2b and S3d–f). When the temperature was set at 750 °C, vertically aligned carbon nanotubes were formed, following the "tip-growth" mechanism (Figs. S2c and S4a–b). The agglomeration of iron nanoparticles could lead to the deposition of carbon layers following the "dissolution–deposition–growth" mechanism. Meanwhile, vertical "tip-growth" mechanism still played a role for growing carbon nanotubes [72]. Interestingly, when the APCVD was performed at 850 °C, porous coral-like iron structures with a smooth surface were formed, which could be ascribed to partial melted individual iron nanoparticles. The agglomeration of iron nanoparticles could absorb maximum 0.022% carbon at 850 °C [21]. The acetylene diffused and dissolved on the surface of Fe (body-centered-cubic structure), then decomposed to active carbon atoms and hydrogen atoms. Once the carbon concentration absorbed in the lattice of Fe reached the maximum value, active carbon atoms deposit along the outside of Fe particles, form hexagonal structure and gradually grow into graphene. With the assistance of high-energy hydrogen atoms and continuous supply of acetylene, large-size and gram-scale graphene sheets were produced (Fig. 3), which is named as the "dissolution–deposition–growth" mechanism. TEM, high-resolution TEM (HRTEM) and selected area electron diffraction (SAED) images in Fig. S5a–d confirmed the proposed growth mechanism. However, when the reaction temperature was further increased to 950 °C, iron nanoparticles melted and formed a large size iron monolith with ladder-like surface structure (Fig. S2d). Meanwhile, body-centered cubic structure of alpha iron was transferred into face-centered cubic structure, inducing a significantly decreased catalytic activity. Only a few carbon fragments were observed (Fig. S2d). The X-ray diffraction (XRD) patterns show the phase changes of the catalysts at different APCVD conditions and different carbon products (Fig. S6).

In order to further verify the optimum temperature for growing graphene, APCVD was also performed at 825 and 875 °C, respectively. We found that graphene sheets and small amount of carbon nanotubes were obtained at 825 °C and

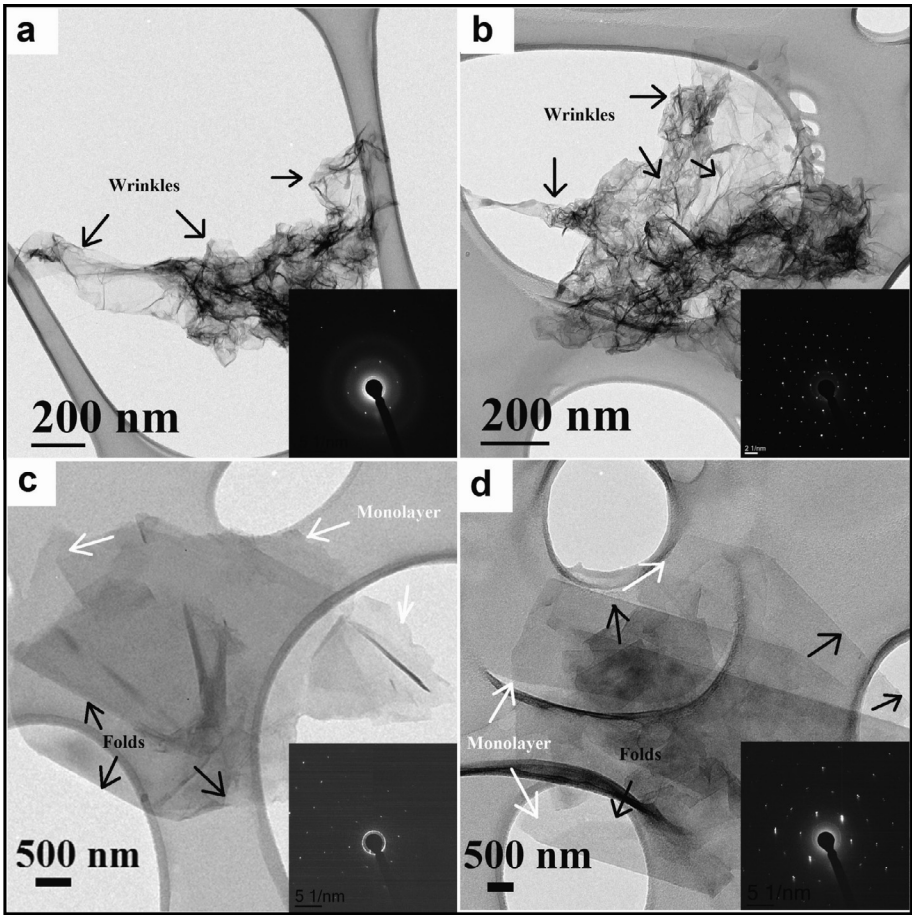

Fig. 4 – TEM images of graphene sheets grown by APCVD at 850 °C with varied growth time. The inset images are the corresponding SAED patterns of graphene sheets. (a) Graphene with wrinkles obtained by APCVD growth for 5 min, pointed by black arrows. (b) Graphene with wrinkles obtained by APCVD growth for 10 min, pointed by black arrows. (c) Graphene with folds obtained by APCVD growth for 30 min, marked by black arrows. The monolayer graphene sheets are labeled by white arrows. (d) Graphene obtained by APCVD growth for 120 min. The folded graphene sheets are annotated by black arrows and monolayer graphene sheets are labeled by white arrows.

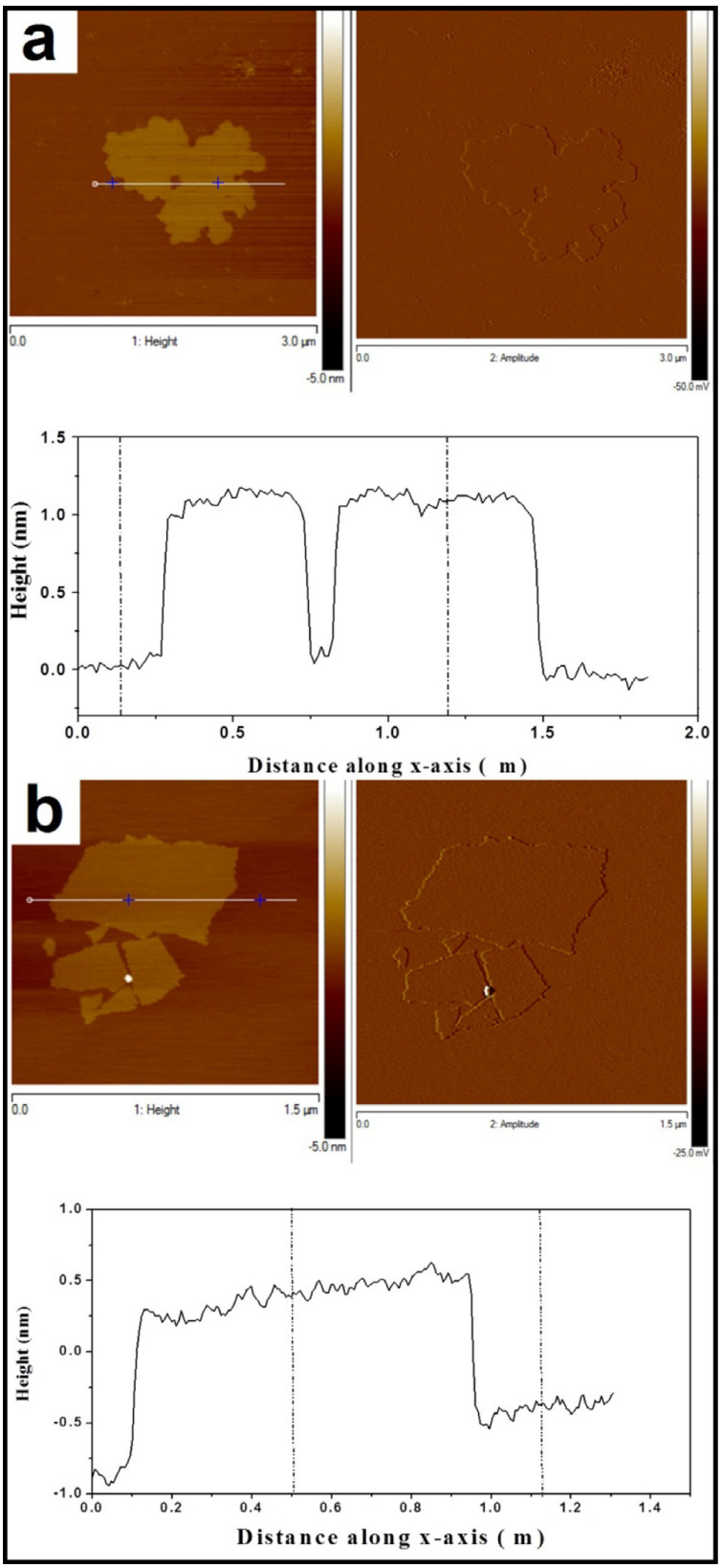

Fig. 5 – AFM images of graphene sheets obtained by tapping mode. The topography, amplitude and height profile are included for each sample. The height profiles obtained from the topography images are marked by white line with Prussian blue cross. Mica discs were used as the substrate. (a) Porous graphene sheets obtained through APCVD growth for 5 min, (b) Crystalline graphene sheets obtained through APCVD deposition for 10 min. (For interpretation of the references to color in this figure legend, the reader is referred to the web version of this article.)

carbon coating phenomenon occurred at 875 °C (Figs. S4c–f and S7a–b, respectively). Therefore, we have determined that 850 °C is the optimum temperature for the growth of graphene under the catalysis of coral-like iron nanoparticles. This temperature is much lower than that catalyzed by Cu [10,13,38,43,73], Ni, Ru and Pt reported previously [17,50,74].

After the identification of the optimum temperature, we investigated the influence of the APCVD reaction time on productivity, crystallinity and size of graphene sheets. Four batches of graphene were synthesized by APCVD at 850 °C for 5, 10, 30 and 120 min, respectively. The graphene products were measured by thermogravimetric analysis (Fig. S10a). Table S1 (supporting information) shows the weight of catalyst and graphene product, from which the C/Fe ration of the as-grown graphene can be determined. Moreover, the percentage of graphene in composites were shown in Fig. S10b, and a Boltzmann curve illustrated the relationship between weight percentage of graphene and growth time, showing that the growth rate was relatively fast in the initial 30 min and became slow subsequently. The products were characterized by FESEM (Fig. S8a–d), TEM and SAED patterns (Fig. 4) and atomic force microscopy (AFM) analysis (Fig. 5). Fig. 4a shows the TEM image of the graphene sheets obtained for 5 min, from which ripples and wrinkles marked by black arrows are clearly visible. One set of sixfold symmetric diffraction spots and two diffraction rings are observed. This indicates that the graphene sheets are single crystalline with some defects. AFM observation determined that the size of graphene sheets is about 2.5 μm^2 with a thickness of 0.9 nm and larger scale scanning area is shown in Fig. S9, exhibiting the average size of graphene is approximate 2 μm^2 by statistics. It should be noted that this batch of graphene sheets has typical zdefects (as shown in Fig. 5a). The defects of graphene sheets may be related to unsufficient supply of carbon source due to short growth time (5 min) and etching effect of hydrogen [50]. When the growth time is prolonged to 10 min, the size of graphene expands to ~3 μm^2 (Fig. 4b) with a thickness of 0.7 nm. As show in the AFM image (Fig. 5b), there is no obvious defects on graphene sheets, even though several larger cavities still exist (Fig. S9b). Fig. 4c–d and Fig. S9c–d show monolayer graphene sheets with some folds, indicating the improvement of the quality.

The crystal structure of the as-synthesized graphene sheets was further analyzed by HRTEM, Fig. 6a shows HRTEM images of monolayer, bi-layer, and triple-layer graphene sheets as well as their corresponding SAED patterns. The HRTEM observation is consistent with SAED identification. For monolayer graphene (Fig. 6a), one set of sixfold symmetric diffraction spots is observed, which is consistant with previous reports [13,39]. The bi-layer graphene presents two sets of sixfold symmetric diffraction spots with a rotation on stacking of 30° between the two layers, and similar report also demonstrates the twisted angles with values between 0° and 30°. The triple-layer graphene sheets exhibit three sets of sixfold symmetric diffraction spots with a rotation of 3° among those diffraction spots. Whereas, if there is no rotation among AB stacked graphene layers, only one set of sixfold symmetric diffraction spots can be detected. Fig. 6b–e show HRTEM images of basal planes of graphene sheets produced in four different batches (5 min, 10 min, 30 min and 120 min, respectively). Fig. 6b exhibits a typical feature of amorphous carbon, indicating graphene has not been well crystallized within 5 min growth time, containing some defects. From Fig. 6c, we can observe the co-existence of zigzag and

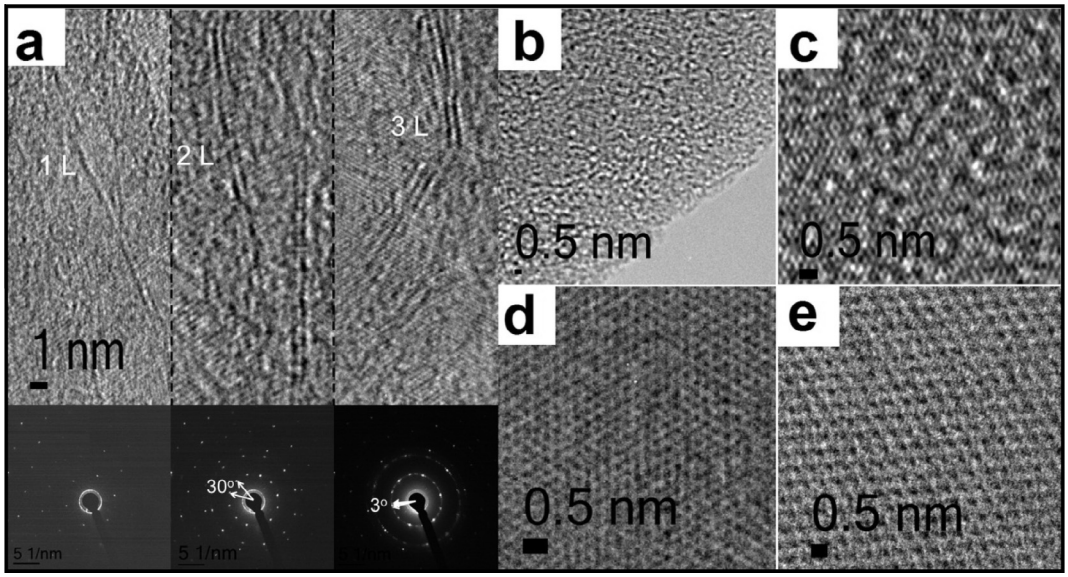

Fig. 6 – HRTEM images of graphene sheets produced by APCVD at 850 °C in different growth times. (a) Graphene sheets with different number of layers and their corresponding SAED patterns. The hexagonal SAED pattern of bilayer graphene shows a rotation in stacking of 30° between two layers and pattern of triple layers graphene exhibits a rotation in stacking of 3°. (b–e) HRTEM images of fine structures of carbon atoms on the basal plane of graphene sheets produced by different APCVD deposition times (b: 5 min, c: 10 min, d: 30 min, e: 120 min), demonstrating improved crystallinity and quality of graphene sheets with the increase of growth time.

arm-chair directions on the basal of graphene synthesized in 10 min. Previous studies claim that the zigzag edges are preferred in graphene grown on polycrystalline metal (Cu) substrate and arm-chair edges may be strongly influenced by CVD condition and electron beam exposure from the microscope [13,75]. As illustrated in Fig. 6d and e, well-crystalline lattices were achieved when the growth durations were extended to 30 min and 120 min, respectively.

The physical and chemical properties of graphene sheets were also characterized by Raman spectra and XPS. Raman spectroscopy is a powerful tool to identify the number of graphene layers and detect amorphous structure [76]. According to the previous reports [77–79], the intensity ratio of G and 2D bands (I_G/I_{2D}) increases with the number of graphene layers. When the value of I_G/I_{2D} is around than 0.5 and the full width at half maxima (FWHM) is less than 50 cm^{-1}, the graphene sheet can be confirmed to be monolayer. An optical microscope image, 40 μm in length, is presented in Fig. 7a. The Raman spectra in Fig. 7b were taken from the location A, B and C, marked in Fig. 7a. The Raman spectrum taken

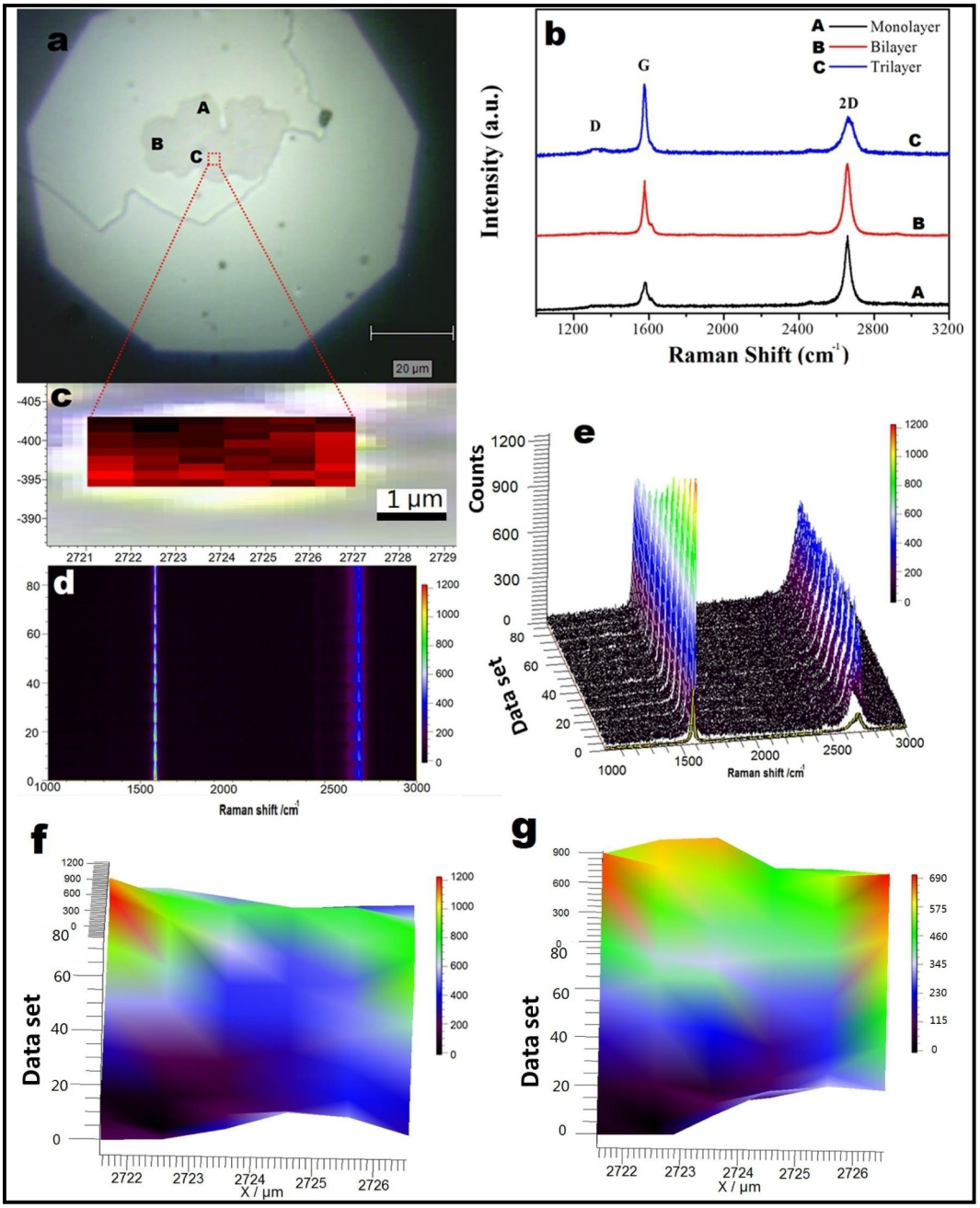

Fig. 7 – (a) An optical microscope image of graphene taken by a Renishaw inVia Raman spectrometer. (b) Raman spectra of monolayer, bilayers and triple layers graphene sheets taken from the location A, B and C marked in (a). (c) An optical microscope image of Raman map of I_G/I_{2G} intensity ratio. (d) Top-view of Raman spectra acquired from the rectangle area in the image (c), showing average FWHM of 35.1 cm^{-1}. (e-g) 3D-view of Raman spectra illustrated by full color, intensity of G band and 2G bands, respectively.

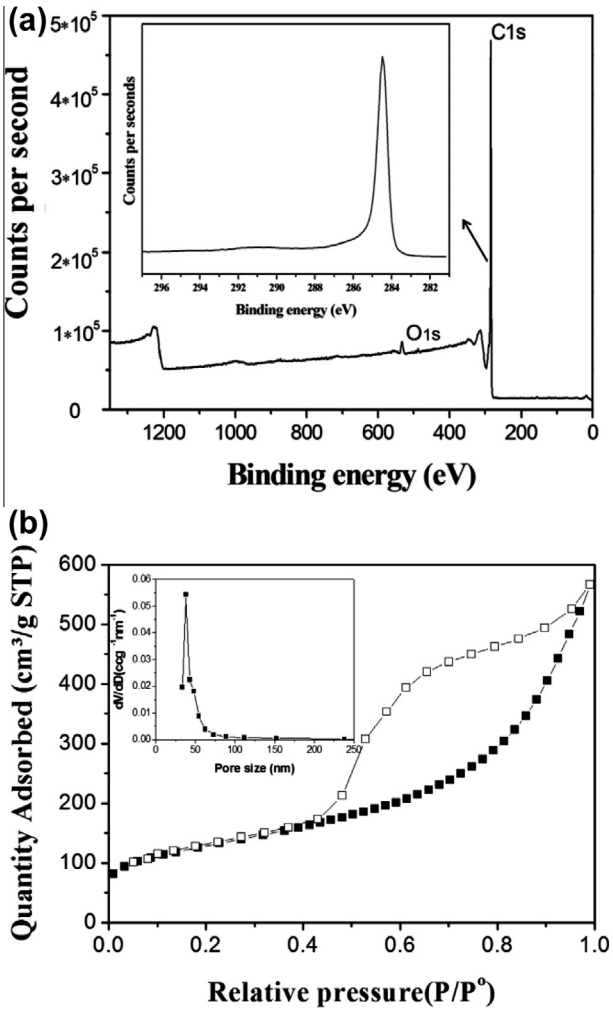

Fig. 8 – X-ray photoelectron spectroscopy spectrum (a) of graphene obtained at 850 °C grown for 30 min. Insert: Peak comes from carbon atoms. The atomic concentration of carbon is more than 99.3%. Nitrogen adsorption/desorption analysis (b) of graphene obtained at 850 °C grown for 30 min. The insert in (b) is the pore size distribution of graphene.

from the location A has the lowest value of I_G/I_{2D} (<0.5), indicating monolayer graphene. The values of I_G/I_{2D} increase at the location B and C, illustrating bilayer and tri-layer graphene or the folded monolayer graphene sheet. Aiming to verify the state of graphene in a continuous area, Raman mapping spectroscopy was acquired from the rectangle part, showing the intensity ration of I_G/I_{2G} in Fig. 7c (related to the thickness of graphene) and the profile of FWHM is shown in Fig. 7d. Larger two-dimensional Raman spectra mappings (Fig. S12a and b) represent the values of I_D/I_G and I_G/I_{2D}, showing coral-like structure and monolayer to triple-layer graphene. The average FWHM is around 35.1 cm^{-1} (an average data statistic calculated from 85 Raman spectra), indicating less apparent defects and amorphous structure. Three-dimensional views of all Raman spectra and intensity of G and 2G bands are shown in Fig. 7e-g, respectively, which can vividly demonstrate the distribution of graphene and intensities of G and 2D bands. Even though the thickness of graphene varies from monolayer to triple-layer, the intensities of 2D band exhibited a constant value, which might be owing to the rotations of graphene sheets (Fig. 6a), which reduced the interlayer coupling effect. The corresponding AFM image after Raman test was shown in Fig. S11. AFM, HRTEM, SAED and Raman spectroscopy analysis clearly confirmed that monolayer to triple-layer graphene sheets have been obtained through the APCVD deposition catalyzed by iron.

XPS spectrum of the graphene sample synthesized by 30 min APCVD deposition is shown in Fig. 8a, demonstrating a sharp C_{1s} peak at 284.2 eV. A small O_{1s} peak is related to the absorbed moisture. The elemental analysis by XPS determined that the graphene sample consists of 99.3% C, 0.51% O and 0.19% Cl (by atomic percentage). The trace Cl is the residual chlorine from dissolving iron catalyst by hydrochloride acid. XPS measurement further proved the high quality of the as-synthesized graphene [80], which was also confirmed by FTIR spectra (Fig. S13). This sample obtained in 30 min

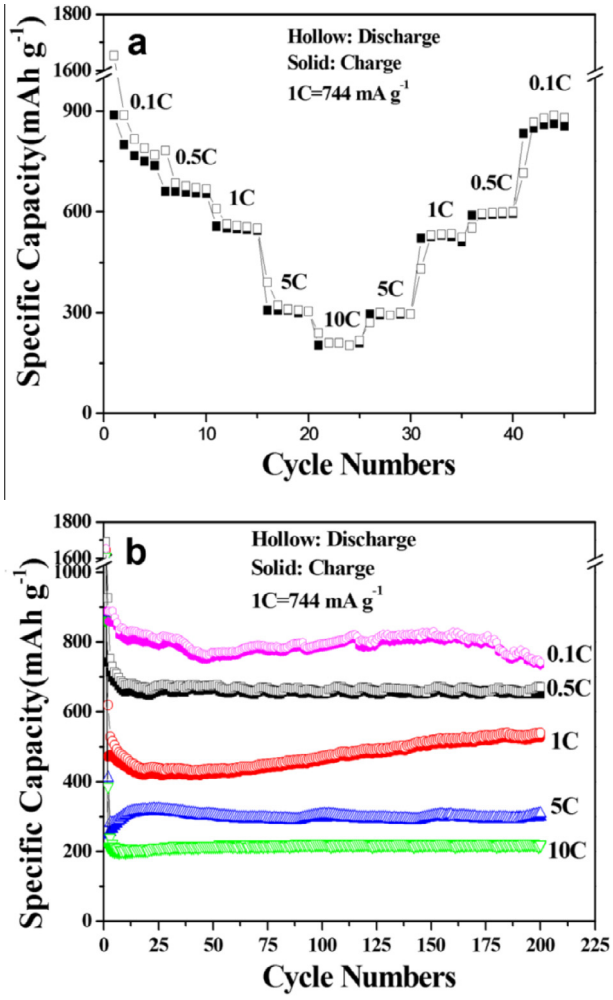

Fig. 9 – The electrochemical performances of graphene sheets. (a) Electrochemical performances of GNS at stepwise current densities. (b) Cycle performances of graphene sheets at different current rates (0.1C, 0.5C, 1C, 5C and 10C, 1C = 744 mA g^{-1}).

was also investigated by nitrogen adsorption and desorption isotherms (Fig. 8b), showing a surface area of 449.2 $m^2 g^{-1}$.

We measured the electrical conductivity, electrochemical behavior and cycle performance of graphene sheets obtained at 850 °C for 30 min. Unlike chemically derived graphene sheets, the APCVD method can successfully avoid oxidization of graphene and produce pure graphene sheets, owing the protection effect of reducing gases. Compared with the electrical conductivities of previously reported chemically derived graphene sheets [15,81], the as-prepared graphene shows a quite high value of ~9.02 S cm^{-1}. The electrochemical reactivity of graphene sheets as anode materials in Li-ion cells was examined by cyclic voltammogram (Fig. S14a). Fig. S14b shows the discharge and charge profiles of graphene anode in the first cycle. Graphene sheets exhibited an initial rechargeable specific capacity of 887 mAh g^{-1} at 0.1C. The irreversible capacity is ascribed to the formation of solid electrolyte interphase. Nevertheless, the cycle performance becomes stable in the following cycles. After 200 cycles, graphene sheets still maintained a capacity of 730 mAh g^{-1}. Even applied with step-wise current densities (0.1C–10C, 1C = 744 mA g^{-1}, Fig. 9a), the graphene electrode can sustain a good cycling performance and high Coulombic efficiency, demonstrating as-synthesized product can tolerate tests with large current densities. Furthermore, graphene sheets exhibited good cycling performances at high current rates (Fig. 9b). In particular, the electrode delivered a lithium storage capacity of more than 560 mAh g^{-1} at 1C rate after 200 cycles, illustrating that the graphene electrode can tolerate high charge and discharge current densities.

4. Conclusions

Monolayer to triple-layer graphene sheets have been successfully prepared by APCVD deposition using acetylene gas as the carbon source and coral-like iron as catalyst. The process can be scaled up for large quantity production at a low cost. The optimum CVD temperature has been identified to be 850 °C. TEM, AFM, Raman spectroscopy and XPS characterizations show the single crystalline and high quality nature of the as-prepared graphene produced by the bottom-up APCVD approach. A new horizontal "dissolution–deposition–growth" mechanism is proposed and verified by TEM and HRTEM analyses. When applied as anode materials in lithium ion batteries, graphene sheets exhibit high initial rechargeable capacity and stable multi-current rate cycling performance. Large scale production of graphene could pave the way for a wide range of applications of graphene materials.

Acknowledgements

This project is financially supported by the Australian Research Council (ARC) through the ARC Discovery project (DP1093855). The author S. Q. Chen gratefully acknowledges the support from the Chinese Scholarship Council (CSC, No. 2011689009). We gratefully acknowledge Dr. Mark Berkahn for assisting AFM measurement.

Appendix A. Supplementary data

Supplementary data associated with this article can be found, in the online version, at http://dx.doi.org/10.1016/j.carbon.2013.07.048.

REFERENCES

[1] Novoselov KS, Geim AK, Morozov SV, Jiang D, Zhang Y, Dubonos SV, et al. Electric field effect in atomically thin carbon films. Science 2004;306(5696):666–9.
[2] Peres NMR, Novoselov KS, Geim AK. The electronic properties of graphene. Rev Mod Phys 2009;324(5934):1530–4.
[3] Geim AK. Graphene: status and prospects. Science 2009;324(5934):1530–4.
[4] Novoselov KS, McCann E, Morozov SV, Fal'ko VI, Katsnelson MI, Zeitler U, et al. Unconventional quantum hall effect and berry's phase of 2π in bilayer graphene. Nat Phys 2006;2(3):177–80.
[5] Huang Y, Liang J, Chen Y. An overview of the applications of graphene-based materials in supercapacitors. Small 2012;8(12):1805–34.
[6] Wang G, Shen X, Yao J, Park J. Graphene nanosheets for enhanced lithium storage in lithium ion batteries. Carbon 2009;47(8):2049–53.
[7] Xiao J, Mei D, Li X, Xu W, Wang D, Graff GL, et al. Hierarchically porous graphene as a lithium–air battery electrode. Nano Lett 2011;11(11):5071–8.
[8] Stoller MD, Park S, Zhu Y, An J, Ruoff RS. Graphene-based ultracapacitors. Nano Lett 2008;8(10):3498–502.
[9] Robinson JT, Perkins FK, Snow ES, Wei Z, Sheehan PE. Reduced graphene oxide molecular sensors. Nano Lett 2008;8(10):3137–40.
[10] Bae S, Kim H, Lee Y, Xu X, Park J-S, Zheng Y, et al. Roll-to-Roll production of 30-inch graphene films for transparent electrodes. Nat Nanotechnol 2010;5(8):574–8.
[11] Li X, Cai W, An J, Kim S, Nah J, Yang D, et al. Large-area synthesis of high-quality and uniform graphene films on copper foils. Science 2009;324(5932):1312–4.
[12] Gao L, Ren W, Zhao J, Ma L-P, Chen Z, Cheng H-M. Efficient growth of high-quality graphene films on cu foils by ambient pressure chemical vapor deposition. Appl Phys Lett 2010;97(18):183109.
[13] Yu Q, Jauregui LA, Wu W, Colby R, Tian J, Su Z, et al. Control and characterization of individual grains and grain boundaries in graphene grown by chemical vapour deposition. Nat Mater 2011;10(6):443–9.
[14] Ismach A, Druzgalski C, Penwell S, Schwartzberg A, Zheng M, Javey A, et al. Direct chemical vapor deposition if graphene in dielectric surfaces. Nano Lett 2010;10(5):1542–8.
[15] Chen Z, Ren W, Gao L, Liu B, Pei S, Cheng H-M. Three-dimensional flexible and conductive interconnected graphene networks grown by chemical vapour deposition. Nat Mater 2011;10(6):424–8.
[16] Reina A, Jia X, Ho J, Nezich D, Son H, Bulovic V, et al. Large area, few-layer graphene films in arbitrary substrates by chemical vapor deposition. Nano Lett 2008;9(1):30–5.
[17] Sutter PW, Flege J-I, Sutter EA. Epitaxial Graphene on Ruthenium. Nat Mater 2008;7(5):406–11.
[18] Pan Y, Zhang H, Shi D, Sun J, Du S, Liu F, et al. Highly ordered, millimeter-scale, continuous, single-crystalline graphene monolayer formed on Ru (0001). Adv Mater 2009;21(27):2777–80.

[19] Shu H, Chen X, Tao X, Ding F. Edge structural stability and kinetics of graphene chemical vapor deposition growth. ACS Nano 2012;6(4):3243–50.
[20] Edwards RS, Coleman KS. Graphene film growth on polycrystalline metals. Acc Chem Res 2012;46(1):23–30.
[21] Xue Y, Wu B, Guo Y, Huang L, Jiang L, Chen J, et al. Synthesis of large-area, few-layer graphene on iron foil by chemical vapor deposition. Nano Res 2011;4(12):1208–14.
[22] Ramón ME, Gupta A, Corbet C, Ferrer DA, Movva HCP, Carpenter G, et al. CMOS-compatible synthesis of large-area, high-mobility graphene by chemical vapor deposition of acetylene on cobalt thin films. ACS Nano 2011;5(9):7198–204.
[23] Zhan N, Wang G, Liu J. Cobalt-assisted large-area epitaxial graphene growth in thermal cracker enhanced gas source molecular beam epitaxy. Appl Phys A 2011;105(2):341–5.
[24] Wang SM, Pei YH, Wang X, Wang H, Meng QN, Tian HW, et al. Synthesis of graphene on a polycrystalline Co film by radio-frequency plasma-enhanced chemical vapour deposition. J Phys D Appl Phys 2010;43(45):455402.
[25] Hummers WS, Offeman RE. Preparation of graphitic oxide. J Am Chem Soc 1958;80(6):1339.
[26] Dreyer DR, Park S, Bielawski CW, Ruoff RS. The chemistry of graphene oxide. Chem Soc Rev 2010;39(1):228–40.
[27] Loh KP, Bao Q, Eda G, Chhowalla M. Graphene oxide as a chemically tunable platform for optical applications. Nat Chem 2010;2(12):1015–24.
[28] Chen S, Chen P, Wu M, Pan D, Wang Y. Graphene supported Sn–Sb@Carbon core-shell particles as a superior anode for lithium ion batteries. Electrochem Commun 2010;12(10):1302–6.
[29] Chen SQ, Wang Y. Microwave-assisted synthesis of a Co_3O_4–Graphene sheet-on-sheet nanocomposite as a superior anode material for Li-Ion batteries. J Mater Chem 2010;20(43):9735–9.
[30] Zhang X, Coleman AC, Katsonis N, Browne WR, van Wees BJ, Feringa BL. Dispersion of graphene in ethanol using a simple solvent exchange method. Chem Commun 2010;46(40):7539–41.
[31] Jiao L, Zhang L, Ding L, Liu J, Dai H. Aligned graphene nanoribbons and crossbars from unzipped carbon nanotubes. Nano Res 2010;3(6):387–94.
[32] Jiao L, Zhang L, Wang X, Diankov G, Dai H. Narrow graphene nanoribbons from carbon nanotubes. Nature 2009;458(7240):877–80.
[33] Kosynkin DV, Higginbotham AL, Sinitskii A, Lomeda JR, Dimiev A, Price BK, et al. Longitudinal unzipping of carbon nanotubes to form graphene nanoribbons. Nature 2009;458(7240):872–6.
[34] Xie L, Wang H, Jin C, Wang X, Jiao L, Suenaga K, et al. Graphene nanoribbons from unzipped carbon nanotubes: atomic structures, raman spectroscopy, and electrical properties. J Am Chem Soc 2011;133(27):10394–7.
[35] Shao Y, Wang J, Wu H, Liu J, Aksay IA, Lin Y. Graphene based electrochemical sensors and biosensors: a review. Electroanal 2010;22(10):1027–36.
[36] Kim KS, Zhao Y, Jang H, Lee SY, Kim JM, Kim KS, et al. Large-scale pattern growth of graphene films for stretchable transparent electrodes. Nature 2009;457(7230):706–10.
[37] Geng D, Wu B, Guo Y, Huang L, Xue Y, Chen J, et al. Uniform hexagonal graphene flakes and films grown on liquid copper surface. Proc Natl Acad Sci USA 2012;109(21):7992–6.
[38] Li X, Magnuson CW, Venugopal A, Tromp RM, Hannon JB, Vogel EM, et al. Large-area graphene single crystals grown by low-pressure chemical vapor deposition of methane on copper. J Am Chem Soc 2011;133(9):2816–9.
[39] Zhang Y, Zhang L, Kim P, Ge M, Li Z, Zhou C. Vapor trapping growth of single-crystalline graphene flowers: synthesis, morphology, and electronic properties. Nano Lett 2012;12(6):2810–6.
[40] Chae SJ, Güneş F, Kim KK, Kim ES, Han GH, Kim SM, et al. Synthesis of large-area graphene layers on poly-nickel substrate by chemical vapor deposition: wrinkle formation. Adv Mater 2009;21(22):2328–33.
[41] Hesjedal T. Continuous roll-to-roll growth of graphene films by chemical vapor deposition. Appl Phys Lett 2011;98(13):133106.
[42] Bhaviripudi S, Jia X, Dresselhaus MS, Kong J. Role of kinetic factors in chemical vapor deposition synthesis if uniform large area graphene using copper catalyst. Nano Lett 2010;10(10):4128–33.
[43] Zhang Y, Gao T, Gao Y, Xie S, Ji Q, Yan K, et al. Defect-like structures of graphene on copper foils for strain relief investigated by high-resolution scanning tunneling microscopy. ACS Nano 2011;5(5):4014–22.
[44] Chen Z, Xu C, Ma C, Ren W, Cheng H-M. Lightweight and flexible graphene foam composites for high-performance electromagnetic interference shielding. Adv Mater 2013;25(9):1296–300.
[45] Zhang Y, Gomez L, Ishikawa FN, Madaria A, Ryu K, Wang C, et al. Comparison of graphene growth on single-crystalline and polycrystalline Ni by chemical vapor deposition. J Phys Chem Lett 2010;1(20):3101–7.
[46] Sinclair R, Itoh T, Chin R. In situ tem studies of metal–carbon reactions. Microsc Microanal 2002;8(04):288–304.
[47] Mattevi C, Kim H, Chhowalla M. A review of chemical vapour deposition of graphene on copper. J Mater Chem 2011;21(10):3324–34.
[48] Zhang Y, Zhang L, Zhou C. Review of chemical vapor deposition of graphene and related applications. Acc Chem Res 2013;10(5):123–43.
[49] Ismach A, Druzgalski C, Penwell S, Schwartzberg A, Zheng M, Javey A, et al. Direct chemical vapor deposition of graphene on dielectric surfaces. Nano Lett 2010;10(5):1542–8.
[50] Sutter P, Sadowski JT, Sutter E. Graphene on Pt(111): growth and substrate interaction. Phys Rev B 2009;80(24):245411.
[51] Wang Y, Zheng Y, Xu X, Dubuisson E, Bao Q, Lu J, et al. Electrochemical delamination of CVD-Grown graphene film: toward the recyclable use of copper catalyst. ACS Nano 2011;5(12):9927–33.
[52] Gao L, Ren W, Xu H, Jin L, Wang Z, Ma T, et al. Repeated growth and bubbling transfer of graphene with millimetre-size single-crystal grains using platinum. Nat Commun 2012;3:699.
[53] Li N, Chen Z, Ren W, Li F, Cheng H-M. Flexible graphene-based lithium ion batteries with ultrafast charge and discharge rates. Proc Natl Acad Sci USA 2012;109(43):17360–5.
[54] Zhou M, Cai T, Pu F, Chen H, Wang Z, Zhang H, et al. Graphene/Carbon-coated Si nanoparticle hybrids as high-performance anode materials for Li-ion batteries. ACS Appl Mater Inter 2013;5(8):3449–55.
[55] Zou Y, Wang Y. Sn@CNT nanostructures rooted in graphene with high and fast Li-storage capacities. ACS Nano 2011;5(10):8108–14.
[56] Wang C, Ju J, Yang Y, Tang Y, Lin J, Shi Z, et al. In situ grown graphene-encapsulated germanium nanowires for superior lithium-ion storage properties. J Mater Chem A 2013;1(31):8897–902.
[57] Bai S, Chen S, Shen X, Zhu G, Wang G. Nanocomposites of hematite ([small alpha]-Fe_2O_3) nanospindles with crumpled reduced graphene oxide nanosheets as high-performance anode material for lithium-ion batteries. R Soc Chem Adv 2012;2(29):10977–84.
[58] Chen S, Bao P, Wang G. Synthesis of Fe_2O_3–CNT–graphene hybrid materials with an open three-dimensional

nanostructure for high capacity lithium storage. Nano Energy 2013;2(3):425–34.
[59] Zou Y, Wang Y. NiO nanosheets grown on graphene nanosheets as superior anode materials for Li-ion batteries. Nanoscale 2011;3(6):2615–20.
[60] Wu Z-S, Zhou G, Yin L-C, Ren W, Li F, Cheng H-M. Graphene/metal oxide composite electrode materials for energy storage. Nano Energy 2012;1(1):107–31.
[61] Yu G, Xie X, Pan L, Bao Z, Cui Y. Hybrid nanostructured materials for high-performance electrochemical capacitors. Nano Energy 2013;2(2):213–34.
[62] Wu QH, Wang C, Ren JG. Sn and SnO2 graphene composites as anode materials for lithium-ion batteries. Ionics 2013;9(19):1–8.
[63] Häglund J. Fixed-spin-moment calculations on bcc and fcc iron using the generalized gradient approximation. Phys Rev B 1993;47(1):566–9.
[64] Sun B, Horvat J, Kim HS, Kim W-S, Ahn J, Wang G. Synthesis of mesoporous α-Fe_2O_3 nanostructures for highly sensitive gas sensors and high capacity anode materials in Lithium ion batteries. J Phys Chem C 2010;114(44):18753–61.
[65] Kondo D, Sato S, Yagi K, Harada N, Sato M, Nihei M, et al. Low-temperature synthesis of graphene and fabrication of top-gated field effect transistors without using transfer processes. Appl Phys Express 2010;3(2):1–3.
[66] Kondo D, Yagi K, Sato M, Nihei M, Awano Y, Sato S, et al. Selective synthesis of carbon nanotubes and multi-layer graphene by controlling catalyst thickness. Chem Phys Lett 2011;514(4):294–300.
[67] An H, Lee W-J, Jung J. Graphene synthesis on Fe foil using thermal CVD. Curr Appl Phys 2011;11(4):S81–5.
[68] He Z, Maurice J-L, Gohier A, Lee CS, Pribat D, Cojocaru CS. Iron catalysts for the growth of carbon nanofibers: Fe, Fe_3C or both? Chem Mater 2011;23(24):5379–87.
[69] Chen S, Chen P, Wang Y. Carbon nanotubes grown *in situ* on graphene nanosheets as superior anodes for Li-ion batteries. Nanoscale 2011;3(10):4323–9.
[70] He M, Liu B, Chernov AI, Obraztsova ED, Kauppi I, Jiang H, et al. Growth mechanism of single-walled carbon nanotubes on iron–copper catalyst and chirality studies by electron diffraction. Chem Mater 2012;24(10):1796–801.
[71] Charlier JC, Amara H, Lambin P. Catalytically assisted tip growth mechanism for single-wall carbon nanotubes. ACS Nano 2007;1(3):202–7.
[72] Guzmán de Villoria R, Hart AJ, Wardle BL. Continuous high-yield production of vertically aligned carbon nanotubes on *2D* and *3D* substrates. ACS Nano 2011;5(6):4850–7.
[73] Gao L, Ren W, Zhao J, Ma L-P, Chen Z, Cheng H-M. Efficient growth of high-quality graphene films on Cu foils by ambient pressure chemical vapor deposition. Appl Phys Lett 2010;97(18):183109–12.
[74] Cui Y, Fu Q, Zhang H, Tan D, Bao X. Dynamic characterization of graphene growth and etching by oxygen on Ru(0001) by photoemission electron microscopy. J Phys Chem C 2009;113(47):20365–70.
[75] Girit ÇÖ, Meyer JC, Erni R, Rossell MD, Kisielowski C, Yang L, et al. Graphene at the edge: stability and dynamics. Science 2009;323(5922):1705–8.
[76] Chen S, Yeoh W, Liu Q, Wang G. Chemical-free synthesis of graphene–carbon nanotube hybrid materials for reversible lithium storage in lithium-ion batteries. Carbon 2012;50(12):4557–65.
[77] Ni ZH, Wang YY, Yu T, Shen ZX. Raman spectroscopy and imaging of graphene. Nano Res 2008;1(4):273–91.
[78] Malard LM, Pimenta MA, Dresselhaus G, Dresselhaus MS. Raman spectroscopy in graphene. Phys Rep 2009;473(5–6):51–87.
[79] Ferrari AC, Meyer JC, Scardaci V, Casiraghi C, Lazzeri M, Mauri F, et al. Raman spectrum of graphene and graphene layers. Phys Rev Lett 2006;97(18):187401–4.
[80] Choucair M, Thordarson P, Stride JA. Gram-scale production of graphene based on solvothermal synthesis and sonication. Nat Nanotech 2009;4(1):30–3.
[81] Ansari S, Kelarakis A, Estevez L, Giannelis EP. Oriented arrays of graphene in a polymer matrix by in situ reduction of graphite oxide nanosheets. Small 2010;6(2):205–9.